NASA TECHNICAL NOTE

NASA TN D-7410

NASA TN D-7410

A RAPID NUMERICAL SOLUTION TO SUBSONIC FLOW OVER PLANAR AND AXISYMMETRIC PROFILES AT AN ANGLE OF ATTACK OF 0°

by Vincent R. Mascitti

Langley Research Center

Hampton, Va. 23665

NATIONAL AERONAUTICS AND SPACE ADMINISTRATION • WASHINGTON, D. C. • MARCH 1974

For sale by the National Technical Information Service, Springfield, Virginia 22151

1. Report No.	2. Government Accession No.	3. Recipient's Catalog No.
NASA TN D-7410		

4. Title and Subtitle	5. Report Date
A RAPID NUMERICAL SOLUTION TO SUBSONIC FLOW OVER PLANAR AND AXISYMMETRIC PROFILES AT AN ANGLE OF ATTACK OF 0°	March 1974
	6. Performing Organization Code

7. Author(s)	8. Performing Organization Report No.
Vincent R. Mascitti	L-8904
	10. Work Unit No. 501-24-05-01

9. Performing Organization Name and Address	11. Contract or Grant No.
NASA Langley Research Center Hampton, Va. 23665	
	13. Type of Report and Period Covered Technical Note

12. Sponsoring Agency Name and Address	14. Sponsoring Agency Code
National Aeronautics and Space Administration Washington, D.C. 20546	

15. Supplementary Notes

16. Abstract

A rapid numerical solution is presented in this paper for the incompressible flow over thin planar and axisymmetric profiles at an angle of attack of 0°. The method uses a finite-difference field solution to the governing equation with a Gauss-Seidel successive overrelaxation scheme. However, the use of a simple Cartesian grid system restricts this method to slender profiles. Results are presented for a cambered airfoil, airfoil in wall effect (two-dimensional flowthrough inlet), body of revolution, and flowthrough nacelle.

A computer program is presented which can be used for any of the previously mentioned cases with simple input changes. Results for compressible flow are available with the use of the appropriate two-dimensional or axisymmetric compressibility corrections. Computational time for a typical field calculation of 3000 grid points and 200 cycles through the field is less than 1 minute with less than 50 000 octal storage on the Control Data Corporation 6600 computing system at the Langley Research Center.

17. Key Words (Suggested by Author(s))	18. Distribution Statement
Subsonic flow Two-dimensional profiles Finite difference	Unclassified – Unlimited STAR Category 01

19. Security Classif. (of this report)	20. Security Classif. (of this page)	21. No. of Pages	22. Price
Unclassified	Unclassified	~~31~~ 34	3.25 ~~3.00~~

A RAPID NUMERICAL SOLUTION TO SUBSONIC FLOW OVER PLANAR AND AXISYMMETRIC PROFILES AT AN ANGLE OF ATTACK OF 0^{o}

By Vincent R. Mascitti
Langley Research Center

SUMMARY

A rapid numerical solution is presented in this paper for the incompressible flow over thin planar and axisymmetric profiles at an angle of attack of 0^{o}. The method uses a finite-difference field solution to the governing equation with a Gauss-Seidel successive overrelaxation scheme. However, the use of a simple Cartesian grid system restricts this method to slender profiles. Results are presented for a cambered airfoil, airfoil in wall effect (two-dimensional flowthrough inlet), body of revolution, and flowthrough nacelle.

A computer program is presented which can be used for any of the previously mentioned cases with simple input changes. Results for compressible flow are available with the use of the appropriate two-dimensional or axisymmetric compressibility corrections. Computational time for a typical field calculation of 3000 grid points and 200 cycles through the field is less than 1 minute with less than 50 000 octal storage on the Control Data Corporation 6600 computing system at the Langley Research Center.

INTRODUCTION

In the past decade the advent of the high-speed digital computer and the development of numerical techniques such as finite differences has enabled the aeronautical researcher to attack many problems which were previously not tractable. Especially in low-speed aerodynamics, a diversity of problems which consider nonlinear effects with inviscid formulations have been approached.

Solutions to the subsonic and transonic flow over airfoils are presented in references 1 and 2. The method of reference 1 is formulated in terms of the velocity potential and rapid computational times are realized even for the transonic flow case. However, extensions of the method to rotational or viscous flow is prohibited. The method of reference 2 was formulated in terms of the stream function, but it was made clear that the stream function formulation is probably not feasible for transonic flow because of the difficulty in evaluating the density function, which becomes double valued in the region of

transonic flow. The transonic flow about slender bodies of revolution was solved in reference 3 with very good accuracy. Once again the velocity potential formulation was utilized. The solution to the transonic nacelle problem was performed in reference 4 by using the streamtube curvature approach.

With these methods available for subsonic and transonic flows, it is appropriate to consider a general solution procedure for subsonic flows which encompasses these profiles and is extendable to rotational and viscous flows.

The purpose of this paper is to present a simple and rapid approach to the generalized two-dimensional (planar or axisymmetric) flow problem requiring the solution of elliptic differential equations. The computer program can be used to reproduce classical incompressible flow solutions, such as the airfoil and body of revolution. But more important, the technique can be used as a springboard for more complex problems in two-dimensional subsonic flow. The program is simple enough to insure that the built-in algorithm for the present governing equation can be replaced with others corresponding to different equations. For example, the rotational flow problem with nonuniform upstream velocity can be solved as in reference 5. A simplified Cartesian grid system which restricts the calculations to slender sections at an angle of attack of 0° is used. Grid refinement in the axial direction is employed to provide a better definition of rapidly changing flow properties. A detailed listing of the computer program with operating instructions is presented.

Illustrations of program applications are presented for cambered airfoil and airfoil with thickness in wall or ground effect, a parabolic body of revolution, and a camber-line nacelle. Results are compared with classical conformal mapping or finite-element singularity solutions. A comparison with experimental data for a NACA series nacelle having thickness and camber, at a Mach number of 0.6 and a mass-flow ratio of 0.787 is also presented to demonstrate the versatility of the method.

SYMBOLS

C_p pressure coefficient

c chord

i,j index for axial and lateral field points (see fig. 1)

K two-dimensional flow index. If = 0, planar; if = 1, axisymmetric

L matrix size

m/m_o mass-flow ratio (the mass flow captured by the profile compared with the flow captured in free stream)

R iteration number

U_o free-stream velocity

u,v velocity components in the z- and r-directions, respectively, nondimensionalized to free-stream velocity

z,r coordinates (see fig. 1)

δ angle corresponding to average trailing-edge slope (positive clockwise, see fig. 1)

ν overrelaxation factor

ψ stream function

ψ_o upstream value of stream function at profile radius

METHOD OF SOLUTION

The governing equation for steady, irrotational, incompressible flow in two dimensions is given in reference 6 as

$$\frac{\partial^2\psi}{\partial r^2} - \frac{K}{r}\frac{\partial\psi}{\partial r} + \frac{\partial^2\psi}{\partial z^2} = 0 \tag{1}$$

If $K = 0$, the flow is planar. If $K = 1$, the flow is axisymmetric. The velocity components are given by:

$$\left.\begin{aligned} u &= -\frac{1}{r^K}\frac{\partial\psi}{\partial r} \\ v &= \frac{1}{r^K}\frac{\partial\psi}{\partial z} \end{aligned}\right\} \tag{2}$$

In the present finite-difference field solution, it was assumed that an infinite field can be represented by a finite field provided that it is sufficiently large compared with the body. Furthermore, along the boundaries of the finite field, the boundary condition at infinity was applied; that is, $v = 0$ and $u = 1$. Therefore

$$\psi_{boundary} \propto r^{K+1}$$

The boundary condition on the surface of the profile is satisfied by

$$\psi_{surface} = \text{Constant}$$

The present method accounts for unequal spacing around a grid point, but for clarity the following equations and algorithms are presented for equal spacing. The finite-difference algorithms for unequal spacing can be readily derived and are presented in appendix A.

The second-order finite-difference algorithm for equations (1) and (2) with equal grid spacing is

$$\frac{1}{\Delta r^2}\left(\psi_{i,j+1} - 2\psi_{i,j} + \psi_{i,j-1}\right) - \frac{K}{2r_j\,\Delta r}\left(\psi_{i,j+1} - \psi_{i,j-1}\right) + \frac{1}{\Delta z^2}\left(\psi_{i+1,j} - 2\psi_{i,j} + \psi_{i-1,j}\right) = 0 \qquad (3)$$

and

$$\left.\begin{aligned} u &= -\frac{1}{2r_j{}^{K}\Delta r}\left(\psi_{i,j+1} - \psi_{i,j-1}\right) \\ v &= \frac{1}{2r_j{}^{K}\Delta z}\left(\psi_{i+1,j} - \psi_{i-1,j}\right) \end{aligned}\right\} \qquad (4)$$

For a given number of grid points L, equation (3) yields L simultaneous linear equations which can be solved by the inversion of an $L \times L$ matrix. However, the resulting influence matrix is strongly diagonal and suggests a solution by iteration.

A possible method is the Gauss-Seidel iteration scheme given by

$$\psi_{i,j}^{R+1} = \frac{1}{\frac{2}{\Delta r^2} + \frac{2}{\Delta z^2}}\left[\frac{1}{\Delta r^2}\left(\psi_{i,j+1}^{R} + \psi_{i,j-1}^{R+1}\right) - \frac{K}{2r_j\,\Delta r}\left(\psi_{i,j+1}^{R} - \psi_{i,j-1}^{R+1}\right) + \frac{1}{\Delta z^2}\left(\psi_{i+1,j}^{R} + \psi_{i-1,j}^{R+1}\right)\right]$$

$$\equiv G\left(\psi_{i,j+1}^{R}, \psi_{i,j-1}^{R+1}, \psi_{i+1,j}^{R}, \psi_{i-1,j}^{R+1}\right) \qquad (5)$$

With this method the calculation marches (fig. 1) from lower left to upper right and continually updates values of the stream function as they become available. The method is convenient to program and requires storage only for L number of points. However, this method was found to converge slowly and required many marches through the field to obtain an accurate solution.

The method selected for this paper employs the Gauss-Seidel overrelaxation scheme given by

$$\psi_{i,j}^{R+1} = \psi_{i,j}^{R} + \nu\left[G\left(\psi_{i,j+1}^{R}, \psi_{i,j-1}^{R+1}, \psi_{i+1,j}^{R}, \psi_{i-1,j}^{R+1}\right) - \psi_{i,j}^{R}\right] \qquad (1 \leq \nu < 2) \qquad (6)$$

Utilizing overrelaxation was found to reduce the number of marches through the field by an order of magnitude over the Gauss-Seidel iteration scheme ($\nu = 1$), as indicated in reference 7 when applied to the Laplace equation.

In the case of a profile where the surface stream function is known a priori (symmetric airfoil and closed body of revolution), the previous equations are sufficient to determine the solution anywhere in the field. For the cases where the stream function ahead of and on the surface is unknown (cambered airfoil, airfoil in ground effect, or nacelle), an additional equation is required. The equation is obtained from the Kutta condition and it is assumed that the flow leaves the trailing edge alined at the average trailing-edge slope. For the trailing edge,

$$-\frac{v}{u} = \tan \delta$$

By using equations (2)

$$\frac{\partial\psi/\partial z}{\partial\psi/\partial r} = \tan \delta$$

by using the appropriate algorithms

$$\frac{1}{\Delta z}\left(-3\psi_{i,j} + 4\psi_{i+1,j} - \psi_{i+2,j}\right) = \frac{\tan \delta}{\Delta r}\left(\psi_{i,j+1} - \psi_{i,j-1}\right)$$

or by rearranging

$$\psi_{i,j} = \frac{1}{3}\left[4\psi_{i+1,j} - \psi_{i+2,j} - \frac{\Delta z}{\Delta r}\tan \delta\left(\psi_{i,j+1} - \psi_{i,j-1}\right)\right] \qquad (7)$$

Equation (7) applies only to the trailing edge. Since the profile is a streamline itself, all profile points can be set equal to $\left(\psi_{i,j}\right)_{\text{trailing edge}}$ and can be continually updated after each sweep through the field.

The grid system incorporated in the present solution can have only one horizontal grid line intersecting the profile. (See fig. 1.) As a result of the simplified grid system employed, this present method is applicable only to slender profiles at an angle of attack of 0°. Naturally, one would not expect accurate results in the region of a blunt leading edge.

The pressure distribution on various profiles is presented in the next section and is compared with classical solutions. The pressure coefficient can be calculated by the following relations:

$$C_p = 1 - \left(u^2 + v^2\right)$$

where

$$u = -\frac{1}{rK}\frac{\partial \psi}{\partial r}$$

$$v = u\left.\frac{dr}{dz}\right|_{\text{surface}}$$

A listing of the computer program used to calculate the field stream function and surface pressures on slender profiles is presented in appendix B. Computational time for obtaining results with this program has been estimated at 1 minute per case for 3000 field points and 200 field sweeps on the Control Data series 6600 computer system at the Langley Research Center.

RESULTS AND DISCUSSION

The present method has been used to compute the flow field and pressure distribution on various profiles. The input field size was enlarged until surface pressures did not vary. Comparisons of results are made with classical or currently used techniques. All cases computed by the present method have required less than 1 minute computational time on the CDC 6600 computer. Computer storage is less than 50 000 octal for all cases. The detailed inputs are presented in appendix B for all cases which were run.

Airfoil With Thickness and Camber

Figure 2 shows the computational grid for the NACA M6 airfoil which has 12-percent-chord thickness and 5.4-percent-chord camber. There are 2091 grid points in the field, the field extends 1 chord length upstream and downstream, and 2 chord lengths laterally.

Figure 3 shows the pressure distribution on the upper and lower surfaces. The solid line represents the solution obtained by using exact potential theory. (See ref. 8.) The symbols show the results obtained by using the present method. In general, agreement is better on the upper surface where there are more grid points near the surface. (See fig. 2.) Agreement is poor near the blunt leading edge where the simplified grid system provides a coarse grid.

Symmetric Airfoil in Wall Effect

Figure 4 shows the computational grid for a symmetric airfoil whose geometry is given by the following relationships:

$$r = 0.025\left[1 - (1 - 2z)^3\right]^{1/3} \qquad (0 \leqq z \leqq 0.5)$$

$$r = 0.025\left[1 - (2z - 1)^3\right] \qquad (0.5 \leqq z \leqq 1)$$

The airfoil has a thickness of 5-percent chord. The wall is placed at 30-percent chord in the lateral direction. There are 2193 grid points in the field.

Figure 5 shows the pressure distribution on the upper and lower surfaces. The solid lines represent the solution using a distribution of surface singularities (ref. 9). The symbols represent the results obtained by using the present method. The agreement is very good for this thinner airfoil except at the blunt leading edge where the grid spacing is too coarse to provide accurate results.

Parabolic Body of Revolution

Figure 6 shows the computational grid for a parabolic body of revolution with 10-percent-chord thickness. The lateral field extends 1.2 chord lengths with 1071 grid points.

Figure 7 shows the pressure distribution on the body surface. The solid line represents the solution obtained by using a distribution of surface singularities. (See ref. 9.) The symbols represent results obtained by using the present method. Once again, the agreement is very good in regions where there are grid points close to the surface.

Camber-Line Nacelle

Figure 8 shows the computational grid for a camber-line nacelle which has 2.135-percent-chord camber and a 13.671-percent-chord capture radius. The lateral field extends 9 capture radii laterally.

Figure 9 shows the pressure distribution on the nacelle surface. The circular symbols are the results obtained by using the streamtube curvature method (ref. 4). The present method, given by the square symbols, shows very good agreement.

NACA 1-89-100 Nacelle

Figure 10 shows the computational grid and geometry of the NACA 1-89-100 nacelle. (See ref. 10.) Experimental data for this nacelle was obtained at a Mach number of 0.6. A translating center body was used in the tests to obtain results for different mass-flow ratios.

The three-dimensional "Gothert" compressibility correction is incorporated in the present method. Because of the simplified grid system the center-body geometry could not be represented. However, results can still be obtained for different mass-flow ratios by deleting the Kutta condition. The Kutta condition or flow direction condition at the trailing edge sets the value of the surface stream function. If the mass flow is known, then the surface stream function is known by

$$\frac{\psi_{surface}}{\psi_0} = \frac{m}{m_0}$$

(See fig. 1.) Since the correct internal geometry is not used, the internal pressure distribution will be invalid. However, the pressure distribution on the outer surface should be correct as long as the proper mass-flow ratio is used.

Figure 11 shows the pressure distribution on the nacelle outer surface at a Mach number of 0.6 and a mass-flow ratio of 0.787. The circular symbols are the experimental data. The square symbols are the values obtained by the present method. The agreement is very good except in the region of the trailing edge, where the proper flow direction because of the presence of the center body is not represented. The example illustrates the versatility of the present method to solve problems which are difficult to handle with classical methods.

CONCLUDING REMARKS

A rapid numerical solution has been presented for the incompressible flow over thin planar and axisymmetric profiles at an angle of attack of 0°. The method uses a finite-difference field solution to the incompressible equation with a Gauss-Seidel successive overrelaxation scheme. In spite of a simplified grid system and a small number of surface points, results were in very good agreement with classical solutions for a variety of cases. The field-point formulation using the stream function is convenient for extending the present capability to subsonic nonpotential inviscid and viscid flows.

Langley Research Center,
National Aeronautics and Space Administration,
Hampton, Va., October 24, 1973.

APPENDIX A

FINITE-DIFFERENCE ALGORITHMS FOR DERIVATIVES WITH UNEQUAL SPACING

For second-order central difference approximations to derivatives of a function across an interval:

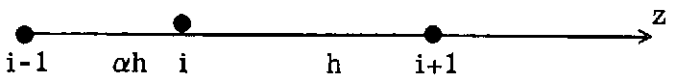

Sketch (a)

the function is of the form

$$\psi = a_0 + a_1 z + a_2 z^2$$

$$\frac{d\psi}{dz} = a_1 + 2a_2 z$$

$$\frac{d^2\psi}{dz^2} = 2a_2$$

because

$$\psi_{i-1} = a_0 \qquad (z = 0)$$

$$\psi_i = \psi_{i-1} + a_1 \alpha h + a_2 \alpha^2 h^2 \qquad (z = \alpha h)$$

$$\psi_{i+1} = \psi_{i-1} + (1 + \alpha) h a_1 + (1 + \alpha)^2 h^2 a_2 \qquad (z = (1 + \alpha)h)$$

where αh and h are relative point spacings. (See sketch (a).) As a result,

$$a_2 = \frac{1}{\alpha h^2 (1 + \alpha)} \left[\psi_{i+1} - (1 + \alpha)\psi_i + \psi_{i-1} \right]$$

$$a_1 = \frac{1}{\alpha h(1+\alpha)}\left[-\alpha^2\psi_{i+1} + (1+\alpha)^2\psi_i - (1+2\alpha)\psi_{i-1}\right]$$

Therefore

$$\left.\frac{d\psi}{dx}\right|_i = \frac{2}{\alpha h(1+\alpha)}\left[\alpha^2\psi_{i+1} + (1+\alpha)(1-\alpha)\psi_i - \psi_{i-1}\right]$$

$$\left.\frac{d^2\psi}{dx^2}\right|_i = \frac{2}{\alpha h^2(1+\alpha)}\left[\alpha\psi_{i+1} - (1+\alpha)\psi_i + \psi_{i-1}\right]$$

APPENDIX B

COMPUTER PROGRAM FOR CALCULATING THE PRESSURE DISTRIBUTION AROUND SLENDER PROFILES

The calculation procedure described in the main body of the paper for obtaining pressure distribution around slender profiles has been programed for high-speed digital computation. The purpose of this appendix is to provide a description of the necessary input and available output as well as a FORTRAN IV (ref. 11) listing of the source program. Input listings for the profiles studied in the main body of the paper are presented. The output listing for the cambered airfoil is presented as an example.

Description of Program

The program reads the profile coordinates and field geometry. The grid is generated and initially labeled as uniform flow. The program marches through the field updating the value of stream function at each point according to the differential equation. At the trailing edge the Kutta condition is used instead of the differential equation. When the field sweep is completed, all profile points are given the same value of stream function as the trailing edge, and a new sweep is started. The program proceeds for 200 sweeps through the field, at which time the surface pressure coefficients are computed with the latest values of stream function. The results are then printed. Computational time for the case of 3000 field points and 200 sweeps through the field is 1 minute. The required storage is 50 000 octal on the CDC 6600 computing system at the Langley Research Center.

Program Listing

The FORTRAN IV listing of the source program used on the Control Data series 6600 computer system at the Langley Research Center is as follows:

```
      DIMENSION XOL(31),YOLT(31),YOLB(31),Z(101),R(81),PSI(101,81),
     1SLOPET(31),SLOPEB(31),DELZ(101),UTAB(41)
      REAL MACH,MASS
      NAMELIST/NUM/XOL,YOLT,YOLB,RBOL,NX,SCALEZ,SCALER,JTE,DELZS,NC,AN
     1,MACH,MASS
  500 READ(5,NUM)
      IF(EOF,5) 200,99
   99 WRITE(6,NUM)
      PI=3.141592653589793
      RBOL=RBOL*SQRT(1.-MACH**2)
      DO 1 I=1,NX
      YOLT(I)=YOLT(I)*SQRT(1.-MACH**2)
    1 YOLB(I)=YOLB(I)*SQRT(1.-MACH**2)
      SCALEZ=SCALEZ+.1E-08
      SCALER=SCALER+.1E-08
C GENERATION OF COMPUTATIONAL GRID
      AL=1.
```

```
      RB=RBOL*AL
      IF(JTE.EQ.1)DELR=.060
      IF(JTE.EQ.1)GO TO 17
      DELR=RBOL/(JTE-1)
   17 CONTINUE
      II=2*NX-1+IFIX((2.*SCALEZ-1.)/DELZS)
      ILE=(II-NX)/2+1
      ITE=ILE+NX-1
      JJ=IFIX((1.+SCALER)*RB/DELR)+1
      IF(JTE.EQ.1)JJ=IFIX(SCALER/DELR)+1
      R(1)=0.
      DO 2 J=2,JJ
    2 R(J)=R(J-1)+DELR
      IMID=(NX-1)/2+1
      DO 30 IB=2,IMID
      I=ILE-IB+1
      DELZ(I)=XOL(IB)-XOL(IB-1)
   30 CONTINUE
      IMF=ILE-(NX-1)/2-1
      DO 31 I=1,IMF
      DELZ(I)=DELZS
   31 CONTINUE
      IMB=ITE+(NX-1)/2
      ILIM=IMB-1
      DO 32 I=ITE,ILIM
      IB=ITE-ILE-(I-ITE)
      DELZ(I)=XOL(IB+1)-XOL(IB)
   32 CONTINUE
      DO 33 I=IMB,II
      DELZ(I)=DELZS
   33 CONTINUE
      K=ITE-1
      DO 35 I=ILE,K
   35 DELZ(I)=XOL(I-ILE+2)-XOL(I-ILE+1)
      Z(1)=0.
      DO 34 I=2,II
   34 Z(I)=Z(I-1)+DELZ(I-1)
C NUMBERING OF BOUNDARY STREAM FUNCTION
      DO 3 I=1,II
      PSI(I,2)=500.
    3 PSI(I,1)=0.
      DO 4 J=2,JJ
      PSI(1,J)=PSI(1,2)*(R(J)/DELR)**NC
      DO 4 I=2,II
    4 PSI(I,J)=PSI(I-1,J)
C FIELD MARCHING LOOPS
      K=II-1
      L=JJ-1
      ICOUNT=0
   10 ICOUNT=ICOUNT+1
      DO 5 J=2,L
      DO 6 I=2,K
      A=1.
      IF((J.EQ.JTE  ).AND.(I.GE.ILE  ).AND.(I.LT.ITE  ))GO TO 6
      IF((J.EQ.JTE).AND.(I.EQ.ITE))GO TO 11
      GO TO 12
   11 IF(MASS.GT.10.)GO TO 15
      PSI(I,J)=PSI(1,JTE)*MASS
      GO TO 6
C KUTTA CONDITION CALCULATION
   15 C=(YOLT(NX-1)-YOLB(NX-1))/(2.*(XOL(NX)-XOL(NX-1)))
      B=DELZ(I+1)/DELZ(I)
      PSI(I,J)=((1.+B)*(1.+B)*PSI(I+1,J)-PSI(I+2,J)-C*B*DELZ(I)*(1.+B)
     1*(PSI(I,J+1)-PSI(I,J-1))/(2.*DELR))/(B*(2.+B))
      IF((J.EQ.JTE).AND.(I.EQ.ITE))GO TO 6
```

```
   12 IF((J.EQ.(JTE+1)).AND.(I.GE.ILE).AND.(I.LE.ITE))GO TO 8
      IF((J.EQ.(JTE-1)).AND.(I.GE.ILE).AND.(I.LE.ITE))
     1A=1.-YOLB(I-ILE+1                )/DELR
      B=DELZ(I)/DELZ(I-1)
      PSI(I,J)=PSI(I,J)+AN*(
     6(PSI(I,J-1)*(2./((1.+A) *DELR*DELR)+A*(NC-1)/((I-1.+A)*DELR*R(J))I+
     1PSI(I,J+1)*(2./(A*(1.+A)*DELR*DELR)-(NC-1)/(A*(I-1.+A)*DELR*R(J))I+
     2(B*PSI(I-1,J)+PSI(I+1,J))*(2./(B*(1.+B)*DELZ(I-1)*DELZ(I-1)))))/
     7(2./(B*DELZ(I-1)*DELZ(I-1))+2./(A*DELR
     3*DELR)-(1.-A)*(NC-1)/(A*DELR*R(J)))
     4-PSI(I,J))
      GO TO 6
    8 A=1.-YOLT(I-ILE+1                )/DELR
      B=DELZ(I)/DELZ(I-1)
      PSI(I,J)=PSI(I,J)+AN*(
     6(PSI(I,J-1)*(2./(A*DELR*DELR*(1.+A))+(NC-1)/(R(J)*A*DELR
     1*(1.+A)))+PSI(I,J+1)*(2./(DELR*DELR*(1.+A))-A*(NC-1)/(R(J)*DELR
     5*(1.+A)))+
     2(B*PSI(I-1,J)+PSI(I+1,J))*(2./(B*(1.+B)*DELZ(I-1)*DELZ(I-1)))))/
     7(2./(B*DELZ(I-1)*DELZ(I-1))+2./(A*DELR*DELR)-(A-1.)*(NC-1)
     3/(R(J)*A*DELR)                   )
     4-PSI(I,J))
    6 CONTINUE
    5 CONTINUE
      DO 9 I=ILE,ITE
    9 PSI(I,JTE)=PSI(ITE,JTE)
      IF(ICOUNT.EQ.200)GO TO 20
      GO TO 10
   20 CONTINUE
      IT=NX-1
      DO 14 I=2,IT
      SLOPET(I)=(YOLT(I+1)-YOLT(I-1))/(XOL(I+1)-XOL(I-1))
   14 SLOPEB(I)=-1.*(YOLB(I+1)-YOLB(I-1))/(XOL(I+1)-XOL(I-1))
      SLOPET(1)=YOLT(2)/XOL(2)
      SLOPEB(1)=-1.*YOLB(2)/XOL(2)
      SLOPET(NX)=-1.*YOLT(NX-1)/(XOL(NX)-XOL(NX-1))
      SLOPEB(NX)=YOLB(NX-1)/(XOL(NX)-XOL(NX-1))
      UO=PSI(1,3)/(2.*R(2)**(NC-1)*DELR)
      IL=ILE
      IT=ITE
      IF(JTE.EQ.1)IL=ILE+1
      IF(JTE.EQ.1)IT=ITE-1
C CALCULATION OF VELOCITY COMPONENTS AND PRESSURE COEFFICIENT
      DO 13 I=IL,IT
      A=1.-YOLT(I-ILE+1                )/DELR
      UZT=1./((R(JTE)+YOLT(I-ILE+1))**(NC-1)     *A*DELR*(1.+A))
     1*(-1.*A**2*PSI(I,JTE+2)+(1.+A)**2*PSI(I,JTE+1)-(1.+2.*A)*
     2PSI(I,JTE))/UO
      URT=UZT*SLOPET(I-ILE+1                )
      UZT=(UZT-1.)/(1.-MACH**2)+1.
      URT=URT/SQRT(1.-MACH**2)
      CPT=1.-(UZT**2+URT**2)
      IF(MACH.GT.0.)CPT=((1.+MACH**2*CPT/5.)**3.5-1.)/(.7*MACH**2)
      IF(JTE.EQ.1)GO TO 18
      A=1.-YOLB(I-ILE+1                )/DELR
      UZB=1./((R(JTE)+YOLB(I-ILE+1))**(NC-1)     *A*DELR*(1.+A))*
     1((1.+2.*A)*PSI(I,JTE)-(1.+A)**2*PSI(I,JTE-1)+A**2*PSI(I,JTE-2))/UO
      URB=UZB*SLOPEB(I-ILE+1                )
      UZB=(UZB-1.)/(1.-MACH**2)+1.
      URB=URB/SQRT(1.-MACH**2)
      CPB=1.-(UZB**2+URB**2)
      IF(MACH.GT..1)CPB=((1.+MACH**2*CPB/5.)**3.5-1.)/(.7*MACH**2)
   18 K=I-ILE+1
      WRITE(6,400)XOL(K),CPT,CPB
  400 FORMAT(2X4HXOL=E12.4,2X4HCPT=E12.4,2X4HCPB=E12.4)
   13 CONTINUE
      GO TO 500
  200 STOP
      END
```

Input

A single case consists of the pressure distribution around a given profile. It is necessary to input the profile and field geometry, planar or axisymmetric code number, value of overrelaxation factor, Mach number, and mass-flow ratio. For the loading routine used in the program, any column except the first may be used on the input cards. A decimal format is used for the input quantities. A description of the required inputs and FORTRAN variables used by the source program are as follows:

FORTRAN variable	Description
$NUM	arbitrary name required by the loading routine to define the input data block
XØL	array name for axial profile coordinates
YØLT	array name for upper surface coordinates
YØLB	array name for lower surface coordinates
RBØL	capture radius in percent of chord
NX	number of surface points input
SCALEZ	axial extent of field in percent of chord
SCALER	lateral extent of field in percent of capture radius
JTE	jth value of approach grid line
DELZS	standard axial increment for far field. Multiple of largest surface axial increment. Must be compatible with SCALEZ
NC	code number for planar or axisymmetric NC = 1 planar NC = 2 axisymmetric
AN	overrelaxation factor $1 \leqq AN < 2$
MACH	free-stream Mach number (use for axisymmetric only)

FORTRAN variable	Description
MASS	mass-flow ratio
$	denotes end of case (column 2)

The system loading subroutine in the program (namelist) is very flexible in that the order of the input cards is unimportant and successive cases can be run by repeating the identification and $NUM cards followed by only the changed parameters and a $card. Experience has shown that 1.85 to 1.95 is a suitable value for the overrelaxation factor AN. The input listing for each of the profiles is given.

Input for NACA M-6 Airfoil

```
$NUM
XOL     =  0.0,  0.125E-01,  0.25E-01,  0.5E-01,  0.75E-01,  0.1E+00,
           0.15E+00,  0.2E+00,  0.3E+00,  0.4E+00,  0.5E+00,  0.6E+00,
           0.7E+00,  0.8E+00,  0.85E+00,  0.9E+00,  0.925E+00,  0.95E+00,
           0.975E+00,  0.9875E+00,  0.1E+01,  1,  1,  1,  1,  1,  1,  1,  1,  1,
YOLT    =  0.0,  0.197E-01,  0.281E-01,  0.403E-01,  0.494E-01,  0.571E-01,
           0.682E-01,  0.755E-01,  0.822E-01,  0.805E-01,  0.726E-01,
           0.603E-01,  0.468E-01,  0.306E-01,  0.23E-01,  0.155E-01,
           0.122E-01,  0.88E-02,  0.44E-02,  0.22E-02,  0.0,  1,  1,  1,  1,  1,  1,
          1,  1,  1,  1,
YOLB    =  0.0,  0.176E-01,  0.22E-01,  0.273E-01,  0.303E-01,  0.324E-01,
           0.347E-01,  0.362E-01,  0.379E-01,  0.39E-01,  0.394E-01,
           0.382E-01,  0.348E-01,  0.283E-01,  0.23E-01,  0.177E-01,
           0.143E-01,  0.109E-01,  0.59E-02,  0.29E-02,  0.0,  1,  1,  1,  1,  1,  1,
          1,  1,  1,  1,
RBOL    =  0.2E+01,
NX      =  21,
SCALEZ  =  0.1E+01,
SCALER  =  0.1E+01,
JTE     =  21,
DELZS   =  0.1E+00,
NC      =  1,
AN      =  0.185E+01,
MACH    =  0.0,
MASS    =  0.2E+02,
$END
```

Input for Airfoil in Wall Effect

```
$NUM
XOL     =  0.0,  0.125E-01,  0.25E-01,  0.5E-01,  0.75E-01,  0.1E+00,
           0.15E+00,  0.2E+00,  0.3E+00,  0.4E+00,  0.5E+00,  0.6E+00,
           0.7E+00,  0.8E+00,  0.85E+00,  0.9E+00,  0.925E+00,  0.95E+00,
           0.975E+00,  0.9875E+00,  0.1E+01,  1,  1,  1,  1,  1,  1,  1,  1,  1,
YOLT    =  0.0,  0.104550528150346E-01,  0.130618661124156E-01,
           0.161781840674016E-01,  0.182007334517046E-01,  0.196824859155116E-01,
           0.217334396335986E-01,  0.230521814602926E-01,  0.244548662325446E-01,
           0.249331547611936E-01,  0.25E-01,  0.248E-01,  0.234E-01,  0.196E-01,
           0.16425E-01,  0.122E-01,  0.964687499999996E-02,
           0.677500000000026E-02,  0.356562499999996E-02,  0.182851562499986E-02,
           0.0,  1,  1,  1,  1,  1,  1,  1,  1,  1,  1,
YOLB    =  0.0,  0.104550528150346E-01,  0.130618661124156E-01,
           0.161781840674016E-01,  0.182007334517046E-01,  0.196824859155116E-01,
           0.217334396335986E-01,  0.230521814602926E-01,  0.244548662325446E-01,
           0.249331547611936E-01,  0.25E-01,  0.248E-01,  0.234E-01,  0.196E-01,
           0.16425E-01,  0.122E-01,  0.964687499999996E-02,
```

```
          0.67750000000002E-02,  0.35656249999999E-02,  0.18285156249998E-02,
          0.0, 1, 1, 1, 1, 1, 1, 1, 1, 1,
 RBOL   = 0.3E+00,
 NX     = 21,
 SCALEZ = 0.1000000001E+01,
 SCALER = 0.6000000001E+01,
 JTE    = 7,
 DELZS  = 0.1E+00,
 NC     = 1,
 AN     = 0.195E+01,
 MACH   = 0.0,
 MASS   = 0.2E+02,
 $END
        0.000 0.000 0.000
        .010  .010  .013
        .013  .013  .025
        .016  .016  .050
        .018  .018  .075
        .020  .020  .100
        .022  .022  .150
        .023  .023  .200
        .024  .024  .300
        .025  .025  .400
        .025  .025  .500
        .025  .025  .600
        .023  .023  .700
        .020  .020  .800
        .016  .016  .850
        .012  .012  .900
        .010  .010  .925
        .007  .007  .950
        .004  .004  .975
        .002  .002  .988
        0.000 0.000 1.000
```

Input for Parabolic Body of Revolution

```
 $NUM
 XOL    = 0.0,  0.125E-01,  0.25E-01,  0.5E-01,  0.75E-01,  0.1E+00,
          0.15E+00,  0.2E+00,  0.3E+00,  0.4E+00,  0.5E+00,  0.6E+00,
          0.7E+00,  0.8E+00,  0.85E+00,  0.9E+00,  0.925E+00,  0.95E+00,
          0.975E+00,  0.9875E+00,  0.1E+01, 1, 1, 1, 1, 1, 1, 1, 1, 1,
 YOLT   = 0.0,  0.246875E-02,  0.4875E-02,  0.95E-02,  0.13875E-01,  0.18E-01,
          0.255E-01,  0.32E-01,  0.42E-01,  0.47999999999999E-01,  0.5E-01,
          0.48E-01,  0.41999999999999E-01,  0.31999999999999E-01,  0.255E-01,
          0.18E-01,  0.13874999999999E-01,  0.94999999999994E-02,
          0.48749999999997E-02,  0.24687499999991E-02,  0.0, 1, 1, 1, 1, 1, 1,
         1, 1, 1, 1,
 YOLB   = 0.0,  0.176E-01,  0.22E-01,  0.273E-01,  0.303E-01,  0.324E-01,
          0.347E-01,  0.362E-01,  0.379E-01,  0.39E-01,  0.394E-01,
          0.382E-01,  0.348E-01,  0.293E-01,  0.23E-01,  0.177E-01,
          0.143E-01,  0.108E-01,  0.59E-02,  0.29E-02,  0.0, 1, 1, 1, 1, 1, 1,
         1, 1, 1, 1,
 RBOL   = 0.0,
 NX     = 21,
 SCALEZ = 0.1000000001E+01,
 SCALER = 0.1200000001E+01,
 JTE    = 1,
 DELZS  = 0.1E+00,
 NC     = 2,
 AN     = 0.195E+01,
 MACH   = 0.0,
 MASS   = 0.0,
 $END
```

```
0.000 0.000 0.000
 .002  .018  .013
 .005  .022  .025
 .009  .027  .050
 .014  .030  .075
 .018  .032  .100
 .025  .035  .150
 .032  .036  .200
 .042  .038  .300
 .048  .039  .400
 .050  .039  .500
 .048  .038  .600
 .042  .035  .700
 .032  .028  .800
 .025  .023  .850
 .018  .018  .900
 .014  .014  .925
 .009  .011  .950
 .005  .006  .975
 .002  .003  .988
0.000 0.000 1.000
36 51 21
 1 .1000
 2 .1000
```

Input for Camber-Line Nacelle

```
$NUM
XOL    =  0.0,  0.125E-01,  0.25E-01,  0.5E-01,  0.75E-01,  0.1E+00,
          0.15E+00,  0.2E+00,  0.3E+00,  0.4E+00,  0.5E+00,  0.6E+00,
          0.7E+00,  0.8E+00,  0.85E+00,  0.9E+00,  0.925E+00,  0.95E+00,
          0.975E+00,  0.9875E+00,  0.1E+01,  1,  1,  1,  1,  1,  1,  1,  1,
YOLT   =  0.0,  0.37E-02,  0.813E-02,  0.1078E-01,  0.1255E-01,  0.1407E-01,
          0.164E-01,  0.1794E-01,  0.1994E-01,  0.2101E-01,  0.2135E-01,
          0.2101E-01,  0.1994E-01,  0.1794E-01,  0.164E-01,  0.1407E-01,
          0.1255E-01,  0.1078E-01,  0.813E-02,  0.37E-02,  0.0,  1,  1,  1,  1,  1,
        1,  1,  1,  1,  1,
YOLB   =  0.0, -0.37E-02, -0.813E-02, -0.1078E-01, -0.1255E-01, -0.1407E-01,
         -0.164E-01, -0.1794E-01, -0.1994E-01, -0.2101E-01, -0.2135E-01,
         -0.2101E-01, -0.1994E-01, -0.1794E-01, -0.164E-01, -0.1407E-01,
         -0.1255E-01, -0.1078E-01, -0.813E-02, -0.37E-02,  0.0,  1,  1,  1,  1,  1,
        1,  1,  1,  1,  1,
RBOL   =  0.13671E+00,
NX     =  21,
SCALEZ =  0.1E+01,
SCALER =  0.9E+01,
JTE    =  5,
DELZS  =  0.5E-01,
NC     =  2,
AN     =  0.185E+01,
MACH   =  0.0,
MASS   =  0.2E+02,
$END
```

Input for NACA 1-89-100 Nacelle

```
$NUM
XOL    =  0.0,  0.125E-01,  0.25E-01,  0.5E-01,  0.1E+00,  0.15E+00,  0.2E+00,
          0.25E+00,  0.3E+00,  0.35E+00,  0.4E+00,  0.45E+00,  0.5E+00,
          0.55E+00,  0.6E+00,  0.65E+00,  0.7E+00,  0.75E+00,  0.8E+00,
          0.85E+00,  0.9E+00,  0.95E+00,  0.975E+00,  0.9875E+00,  0.1E+01,
YOLT   =  0.0,  0.413E-02,  0.604E-02,  0.863E-02,  0.1229E-01,  0.1488E-01,
          0.1675E-01,  0.1808E-01,  0.1885E-01,  0.1904E-01,  0.1904E-01,
          0.1904E-01,  0.1904E-01,  0.1904E-01,  0.1904E-01,  0.1904E-01,
```

```
          0.1904E-01,  0.1894E-01,  0.1796E-01,  0.1577E-01,  0.1227E-01,
          0.717E-02,  0.375E-02,  0.179E-02,  0.0,
YOLB   =  0.0, -0.19E-03, -0.4E-03, -0.85E-03, -0.163E-02, -0.21E-02,
         -0.296E-02, -0.446E-02, -0.638E-02, -0.75E-02, -0.75E-02, -0.75E-02,
         -0.75E-02, -0.75E-02, -0.75E-02, -0.75E-02, -0.75E-02, -0.75E-02,
         -0.75E-02, -0.748E-02, -0.531E-02, -0.152E-02, -0.46E-03, -0.17E-03,
          0.0,
RBOL   =  0.15404E+00,
NX     =  25,
SCALEZ =  0.1E+01,
SCALER =  0.9E+01,
JTE    =  8,
DELZS  =  0.1E+00,
NC     =  2,
AN     =  0.185E+01,
MACH   =  0.6E+00,
MASS   =  0.787E+00,
$END
```

Output

The output listing consists of the upper and lower surface pressure coefficient. A sample output listing is presented for the cambered airfoil case.

```
XOL=  0.           CPT= -2.6676E-01  CPB= -9.4951E-01
XOL=  1.2500E-02   CPT= -5.2217E-01  CPB= -9.4963E-01
XOL=  2.5000E-02   CPT= -6.5589E-02  CPB= -2.7860E-01
XOL=  5.0000E-02   CPT= -2.2225E-01  CPB= -3.1979E-01
XOL=  7.5000E-02   CPT= -3.1975E-01  CPB= -3.0826E-01
XOL=  1.0000E-01   CPT= -4.0671E-01  CPB= -2.9054E-01
XOL=  1.5000E-01   CPT= -5.2227E-01  CPB= -2.3902E-01
XOL=  2.0000E-01   CPT= -5.4801E-01  CPB= -2.0228E-01
XOL=  3.0000E-01   CPT= -5.5010E-01  CPB= -1.6511E-01
XOL=  4.0000E-01   CPT= -4.6875E-01  CPB= -1.5988E-01
XOL=  5.0000E-01   CPT= -3.5354E-01  CPB= -1.7272E-01
XOL=  6.0000E-01   CPT= -2.1705E-01  CPB= -1.8157E-01
XOL=  7.0000E-01   CPT= -1.3615E-01  CPB= -1.8044E-01
XOL=  8.0000E-01   CPT= -7.0207E-03  CPB= -1.5245E-01
XOL=  8.5000E-01   CPT=  4.1780E-02  CPB= -9.9609E-02
XOL=  9.0000E-01   CPT=  9.4420E-02  CPB= -6.4675E-02
XOL=  9.2500E-01   CPT=  1.1362E-01  CPB= -3.1043E-02
XOL=  9.5000E-01   CPT=  1.3221E-01  CPB= -1.2843E-03
XOL=  9.7500E-01   CPT=  1.8229E-01  CPB=  6.3561E-02
XOL=  9.8750E-01   CPT=  2.1151E-01  CPB=  1.0825E-01
XOL=  1.0000E+00   CPT=  2.4196E-01  CPB=  1.5993E-01
```

REFERENCES

1. Jameson, Antony: Transonic Flow Calculations for Airfoils and Bodies of Revolution. Rep. 390-71-1, Grumman Aerospace Corp., 1971.

2. Steger, Joseph Leo: Application of Cyclic Relaxation Procedures to Transonic Flow Fields. Ph. D. Diss., Iowa State Univ., 1969.

3. Bailey, Frank R.: Numerical Calculation of Transonic Flow About Slender Bodies of Revolution. NASA TN D-6582, 1971.

4. Keith, J. S.; Ferguson, D. R.; Merkle, C. L.; Heck, P. H.; and Lahti, D. J.: Analytic Method for Predicting the Pressure Distribution About a Nacelle at Transonic Speeds. NASA CR-2217, 1973.

5. Chow, F.; Krause, E.; Liu, C. H.; and Mao, J.: Numerical Investigations of an Airfoil in a Nonuniform Stream. J. Aircraft, vol. 7, no. 6, Nov.-Dec. 1970, pp. 531-537.

6. Shapiro, Ascher H.: The Dynamics and Thermodynamics of Compressible Fluid Flow. Vol. I. Ronald Press Co., 1958.

7. Ames, William F.: Numerical Methods for Partial Differential Equations. Barnes & Noble, Inc., c.1969.

8. Theodorsen, Theodore; and Garrick, I. E.: General Potential Theory of Arbitrary Wing Sections. NACA Rep. 452, 1933.

9. Hess, J. L.; and Smith, A. M. O.: Calculation of Potential Flow About Arbitrary Bodies. Progress in Aeronautical Sciences, Vol. 8, D. Küchemann, P. Carrière, B. Etkin, W. Fiszdon, N. Rott, J. Smolderen, I. Tani, and W. Wuest, eds., Pergamon Press, Inc., c.1967, pp. 1-138.

10. Re, Richard J.: An Investigation of Several NACA 1-Series Axisymmetric Inlets at Mach Numbers From 0.4 to 1.29. NASA TM X-2917, 1974.

11. McCracken, Daniel D.: A Guide to FORTRAN Programming. John Wiley & Sons, Inc., c.1961.

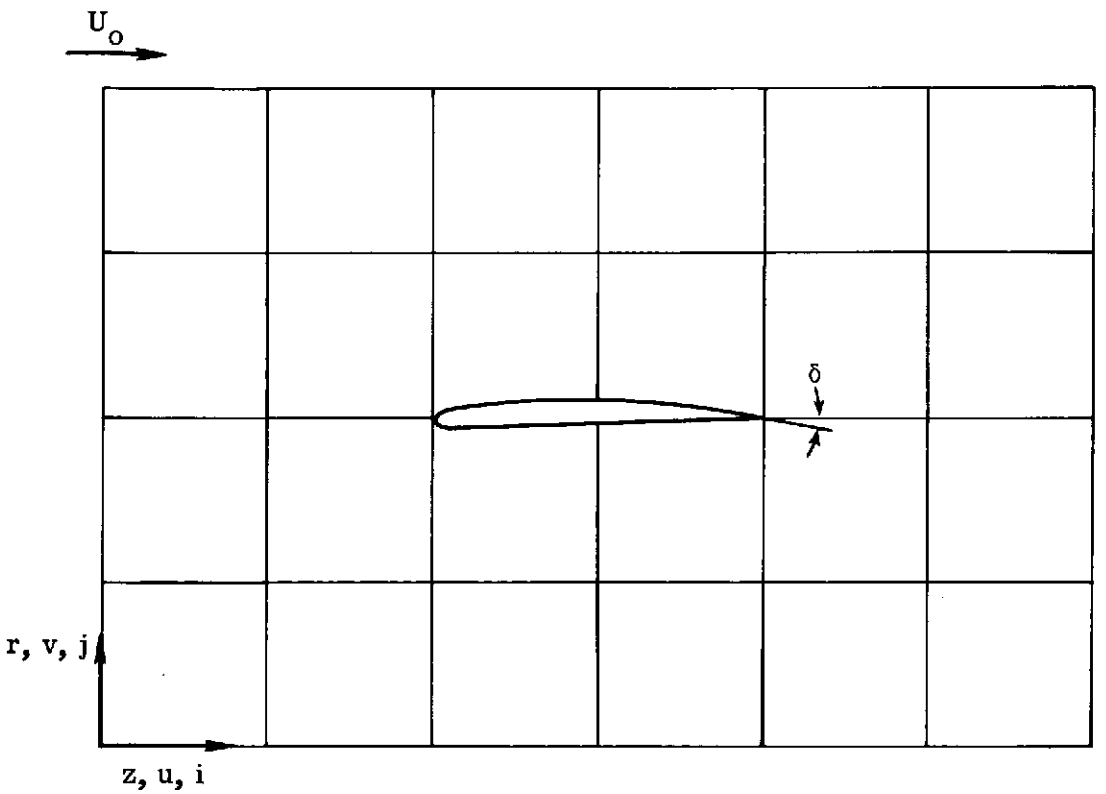

Figure 1.- Field description.

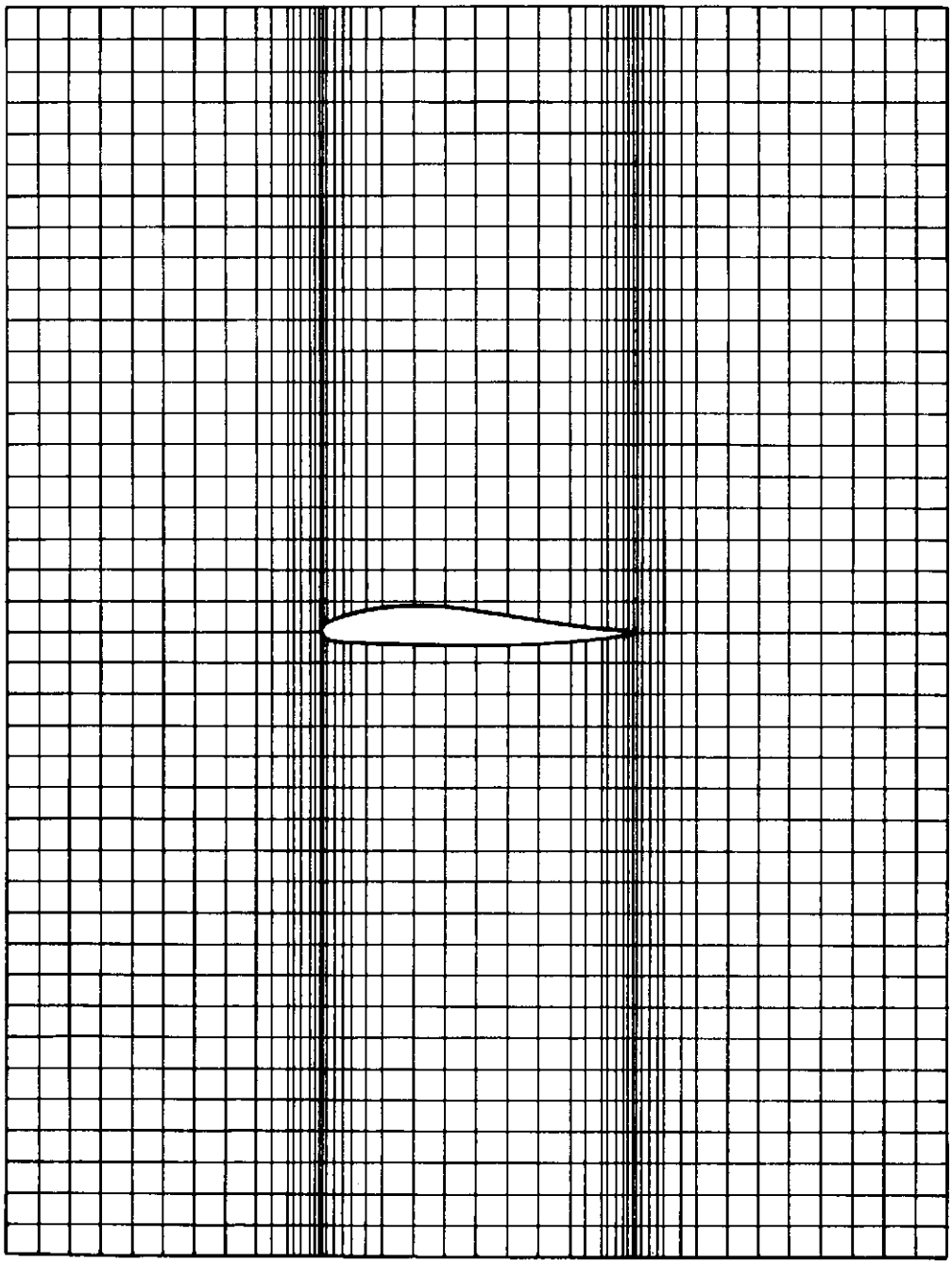

Figure 2.- Computational grid for NACA M6 airfoil.

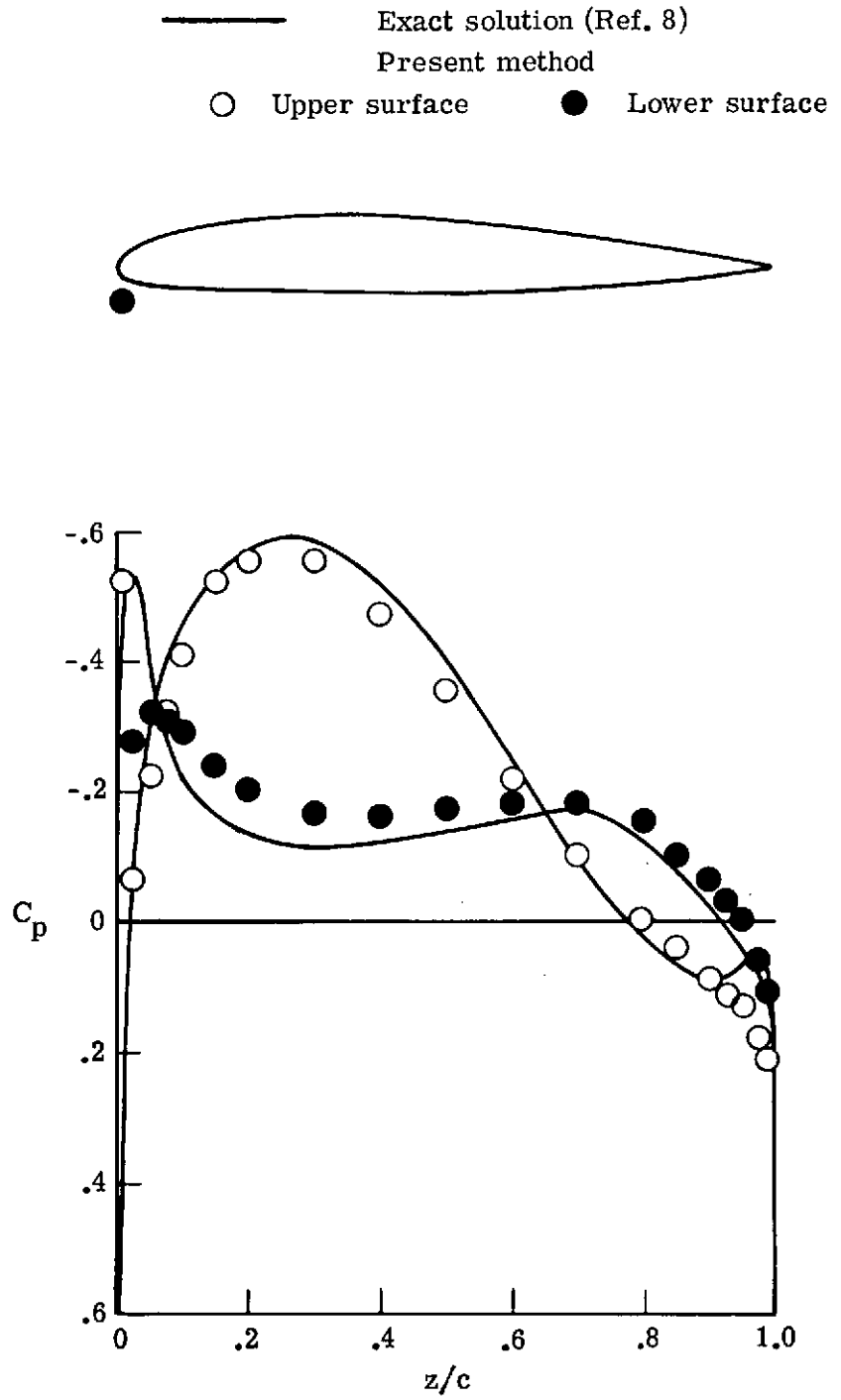

Figure 3.- Pressure distribution on NACA M6 airfoil.

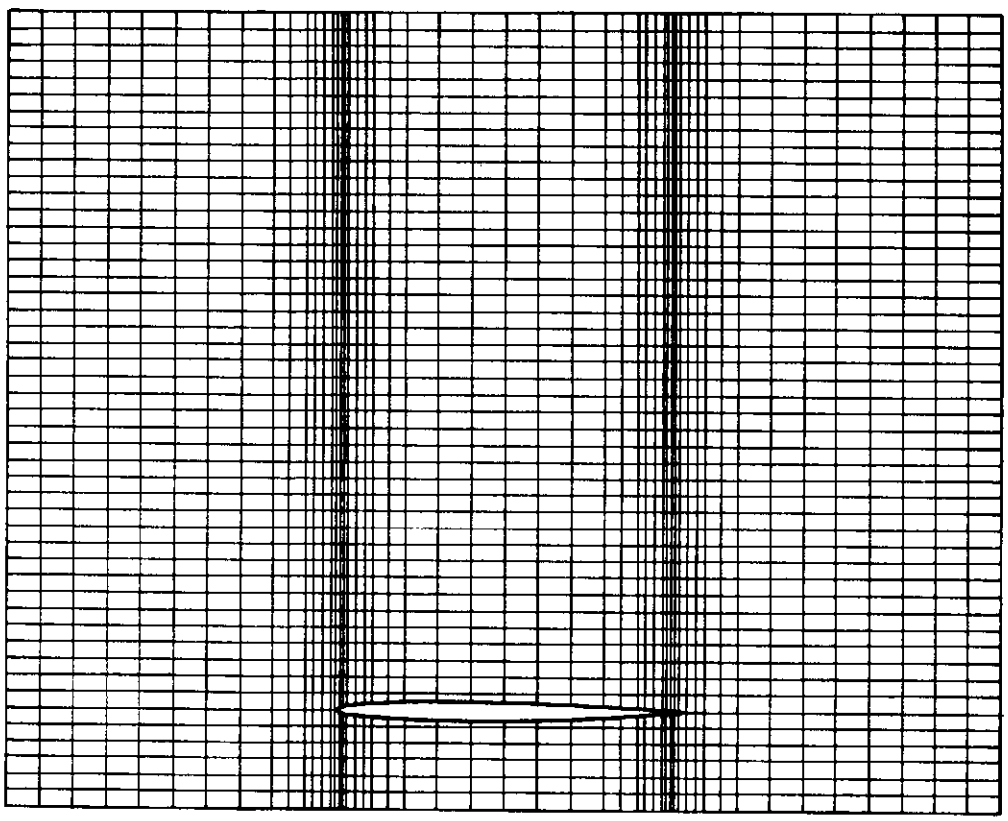

Figure 4.- Computational grid for airfoil in wall effect.

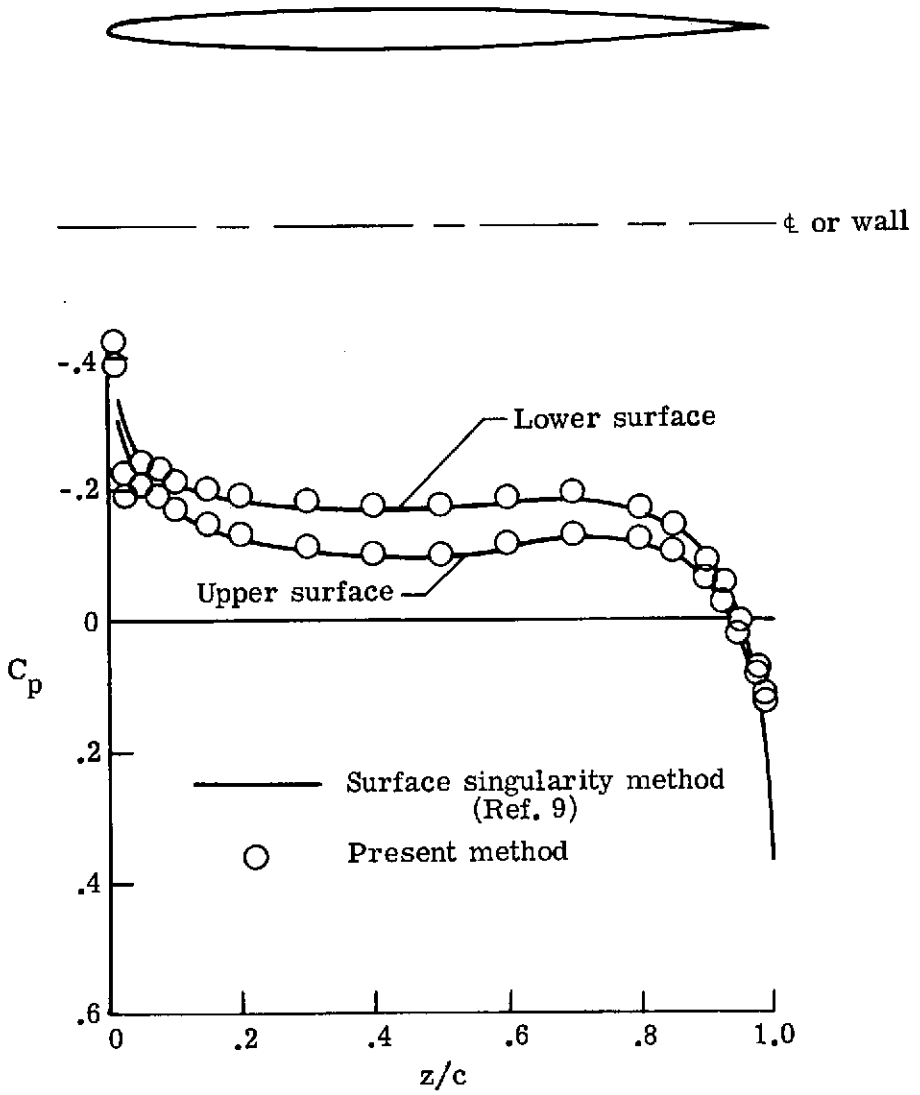

Figure 5.- Pressure distribution on airfoil in wall effect.

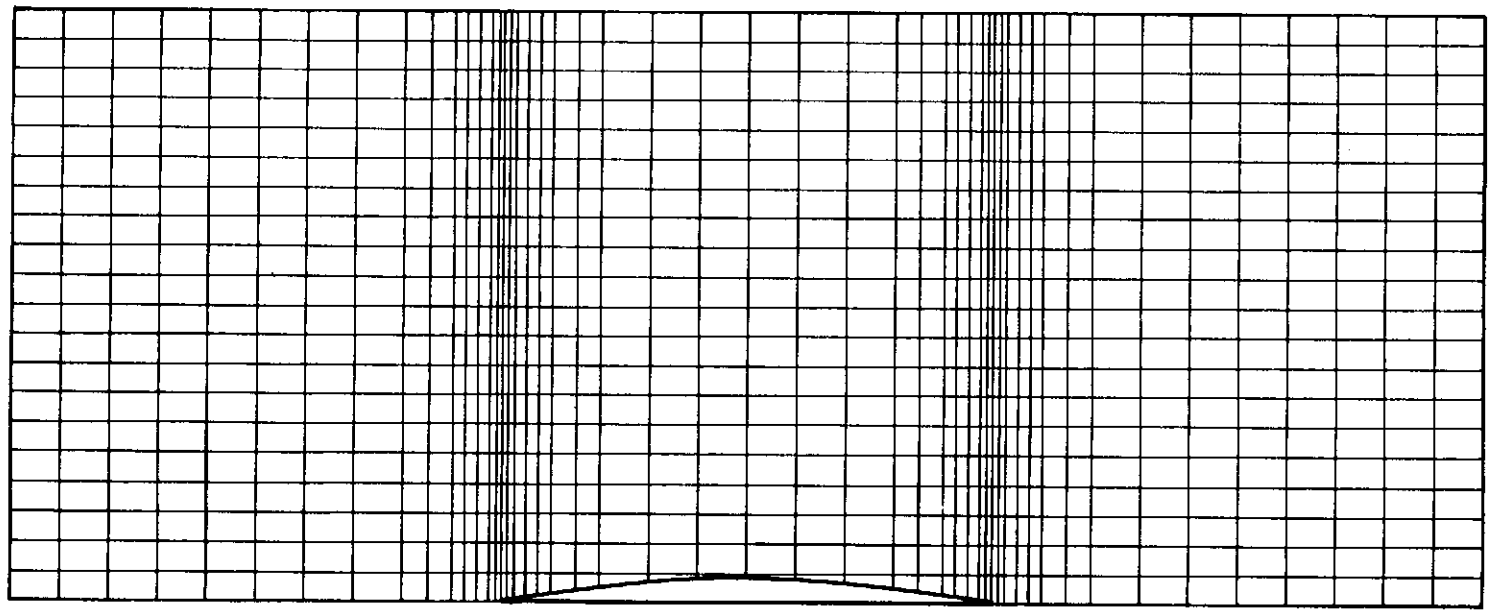

Figure 6.- Computational grid for parabolic body of revolution.

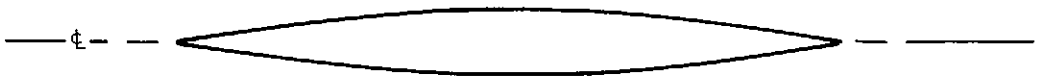

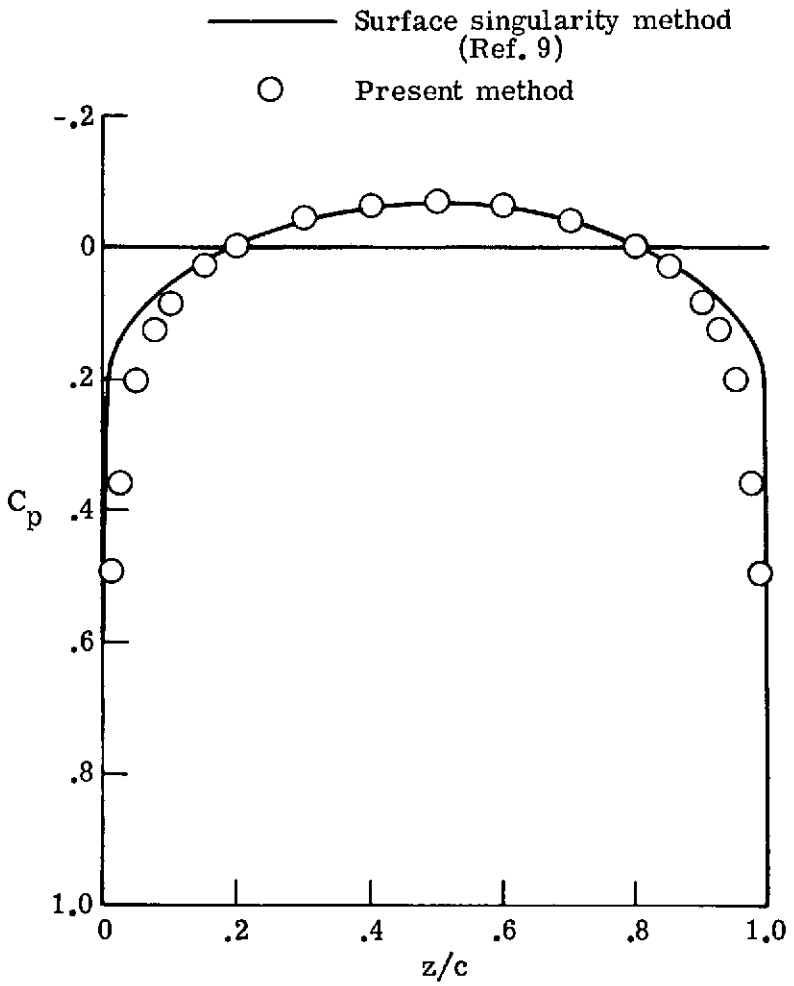

Figure 7.- Pressure distribution on parabolic body of revolution.

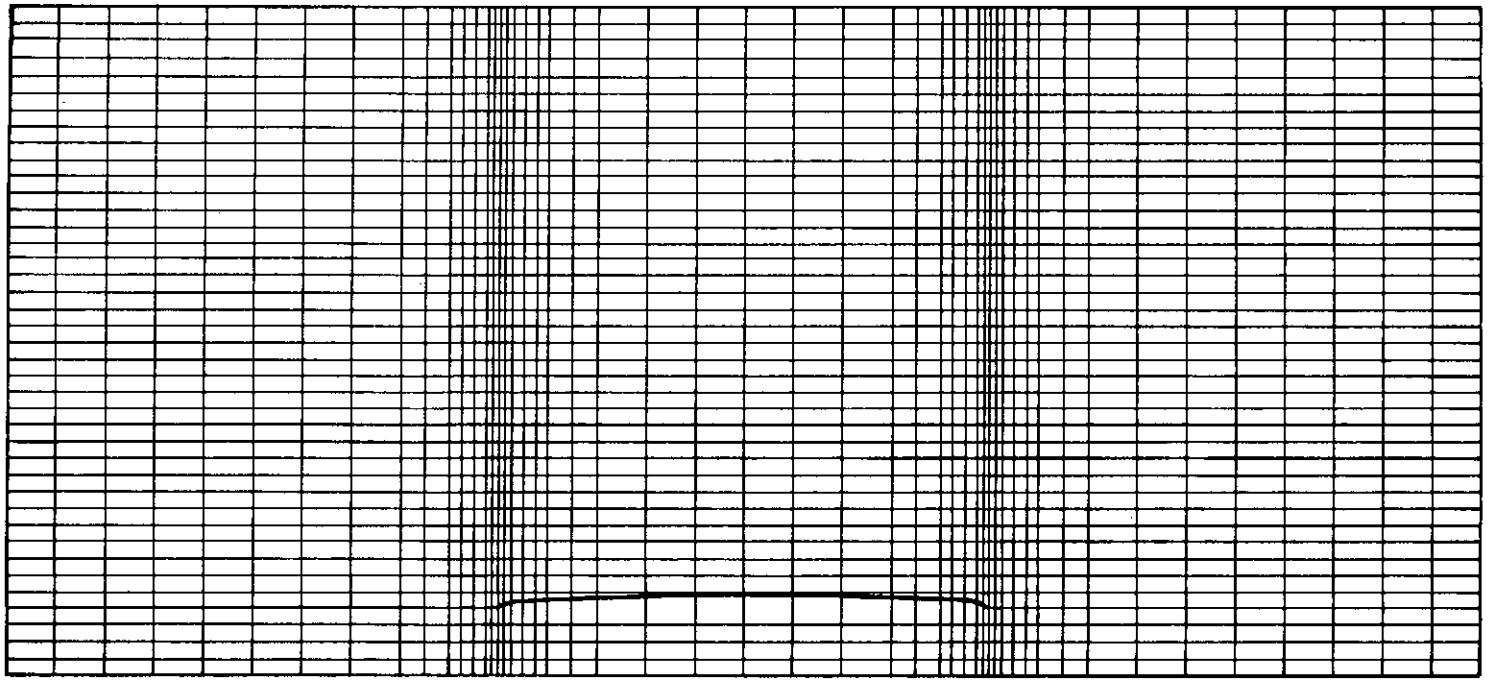

Figure 8.- Computational grid for camber-line nacelle.

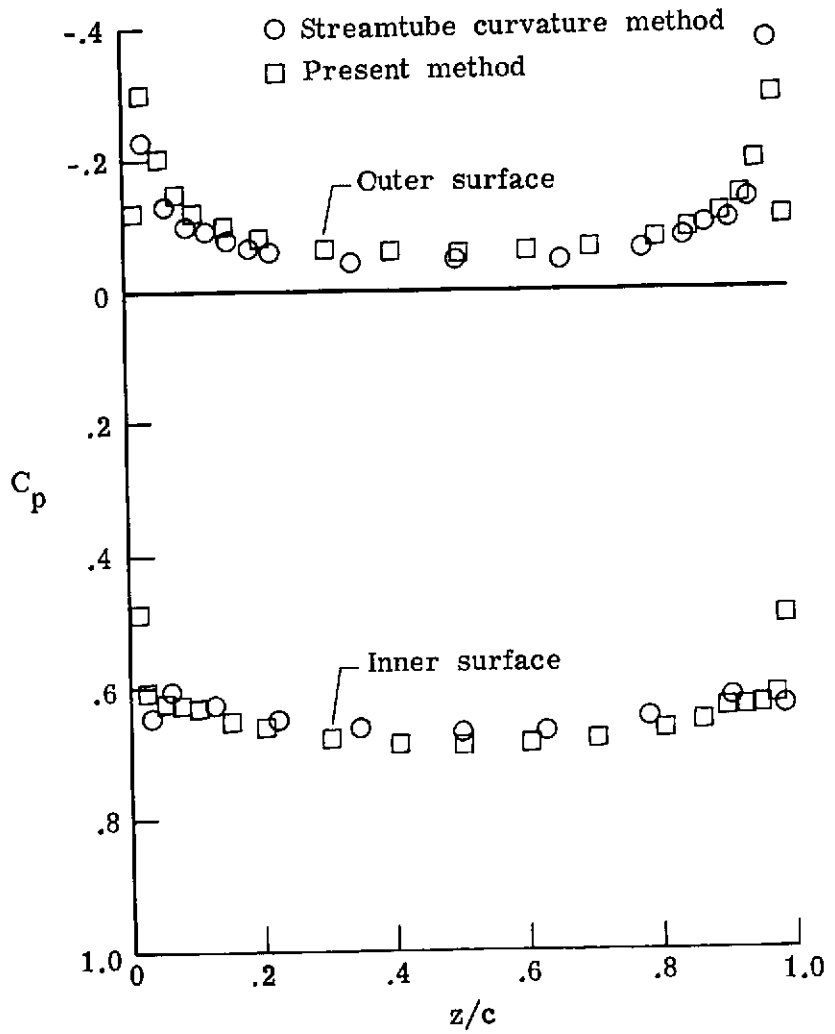

Figure 9.- Pressure distribution on camber-line nacelle.

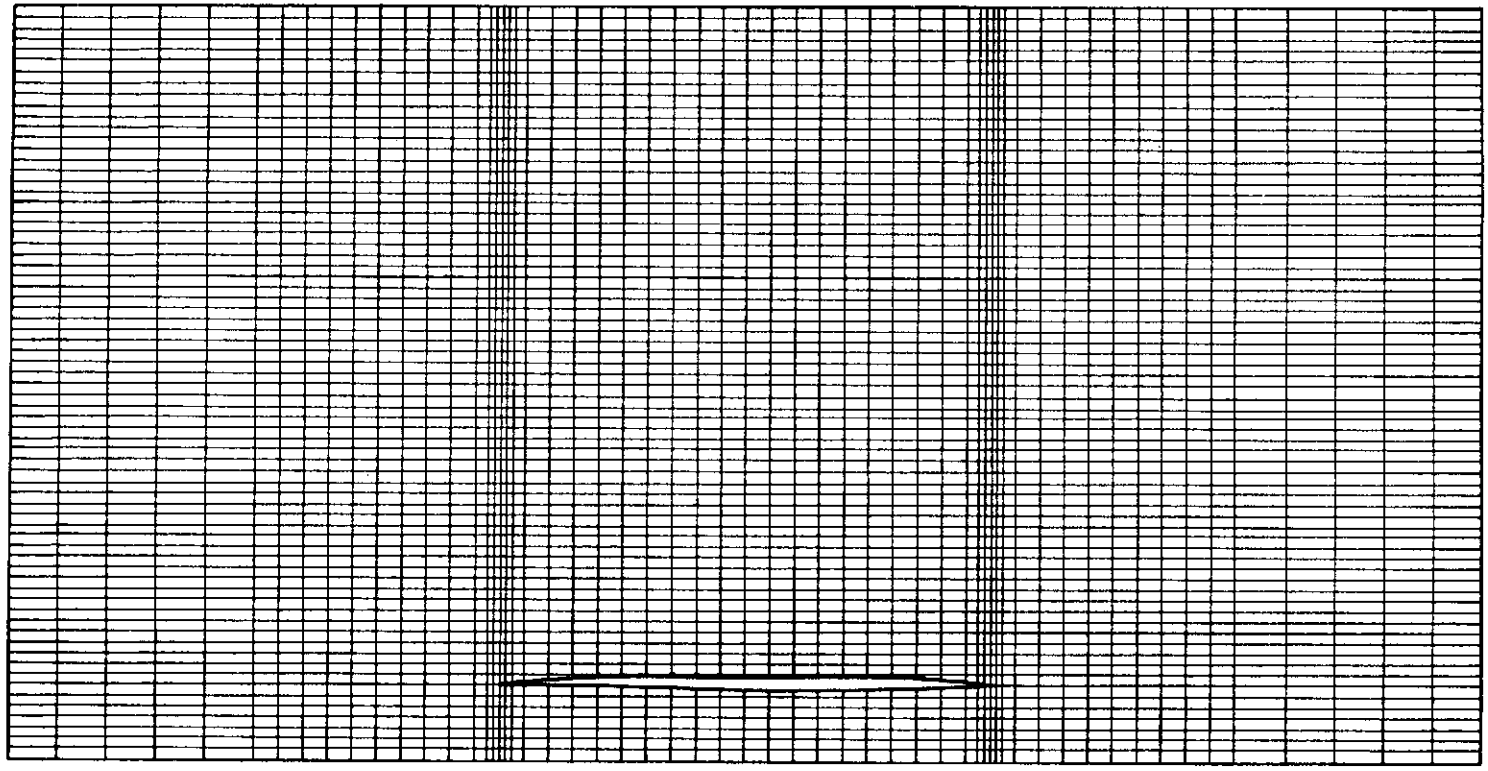

Figure 10.- Computational grid for NACA 1-89-100 nacelle.

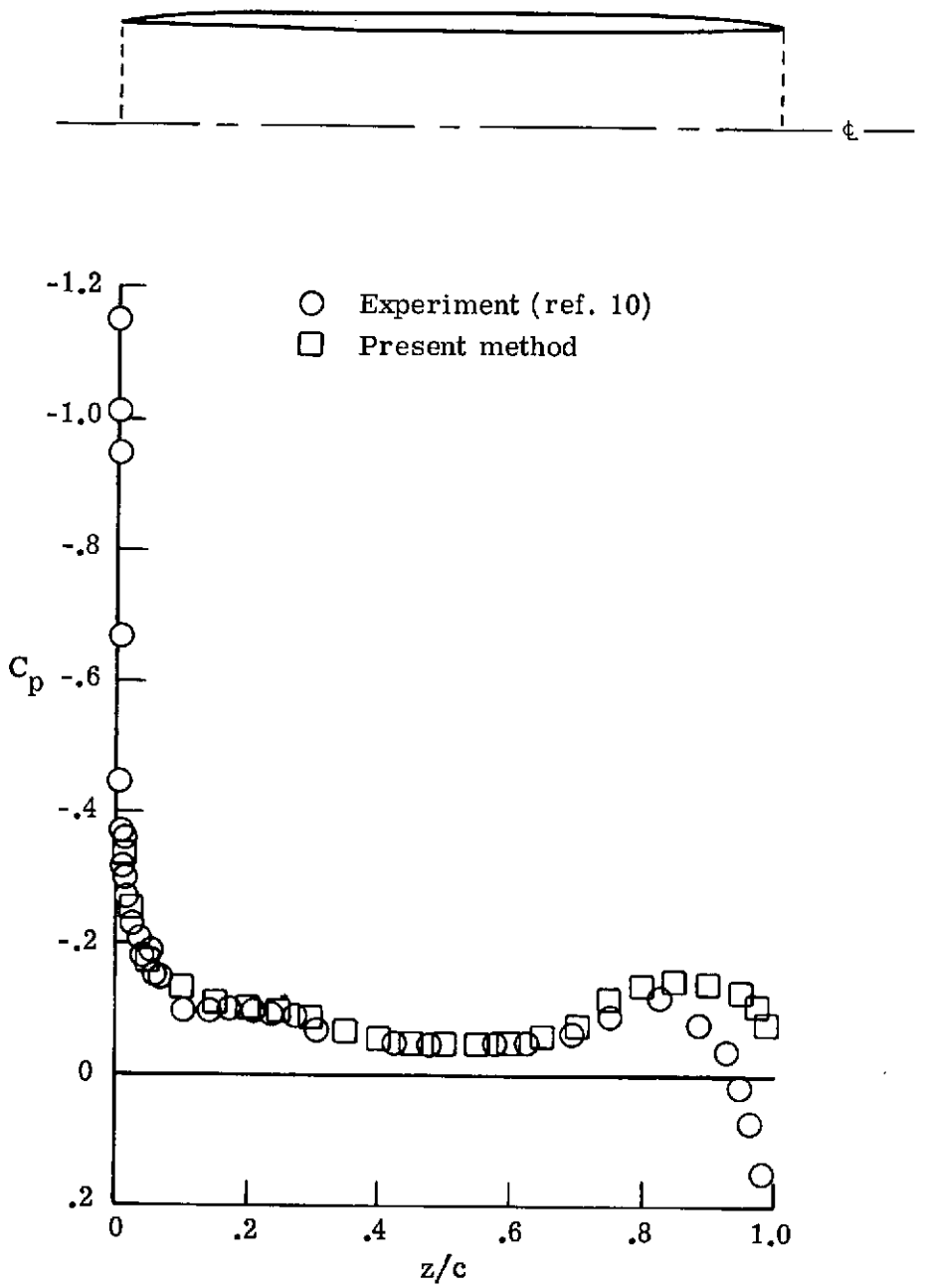

Figure 11.- Pressure distribution on outer surface of NACA 1-89-100 nacelle. M = 0.6; m/m_o = 0.787.